

Microstructure design for fast oxygen conduction

Dilpuneet S. Aidhy^{a)}

Department of Mechanical Engineering, University of Wyoming, Laramie, Wyoming 82071, USA; and Materials Science and Technology Division, Oak Ridge National Laboratory, Oak Ridge, Tennessee 37831, USA

William J. Weber^{b)}

Materials Science and Engineering, University of Tennessee, Knoxville, Tennessee 37996, USA; and Materials Science and Technology Division, Oak Ridge National Laboratory, Oak Ridge, Tennessee 37831, USA

(Received 29 June 2015; accepted 6 October 2015)

In the past decade, the research in designing fast oxygen conducting materials for electrochemical applications has largely shifted to microstructural features, in contrast to material-bulk. In particular, understanding oxygen energetics in heterointerface materials is currently at the forefront, where interfacial tensile strain is being considered as the key parameter in lowering oxygen migration barriers. Nanocrystalline materials with high densities of grain boundaries have also gathered interest that could possibly allow leverage over *excess volume* at grain boundaries, providing fast oxygen diffusion channels similar to those previously observed in metals. In addition, near-interface phase transformations and misfit dislocations are other microstructural phenomenon/features that are being explored to provide faster diffusion. In this review, the current understanding on oxygen energetics, i.e., thermodynamics and kinetics, originating from these microstructural features is discussed. Experimental observations, theoretical predictions and novel atomistic mechanisms relevant to oxygen transport are highlighted. In addition, the interaction of dopants with oxygen vacancies in the presence of these new microstructural features, and their future role in the design of future fast-ion conductors, is outlined.



Dilpuneet S. Aidhy

Dilpuneet Aidhy received his Ph.D. in materials science and engineering from the University of Florida in Spring 2009. He did postdoc at Northwestern University and Argonne National Laboratory between 2009–2011 before joining IBM as a staff scientist. He later joined Oak Ridge National Laboratory as a postdoc in October 2012. Since August 2015, he is working as a tenure-track Assistant Professor at the University of Wyoming, Laramie in the mechanical department. His work focuses on computational microstructure science using atomistic and electronic modeling of point defects, grain boundaries and heterointerfaces in oxide and metallic materials. His primary interests are in oxygen transport in fuel cells, interfacial chemistry, materials design, and radiation effects in materials.

I. INTRODUCTION

Over the past 15 years, materials interfaces have emerged as one of the most intriguing materials design parameters.^{1–9} They possess rich physics and show a variety of strikingly novel properties spread across

diverse applications.^{3,5,7,10–12} For example, interfacing LaAlO₃ (LAO) with SrTiO₃ (STO) unravels magnetism between the two non-magnetic oxides,¹³ and engenders the coexistence of ferromagnetism and superconductivity.¹⁴ Similarly, interfacing can significantly increase transition temperatures as evidenced in superconducting La_{2–x}Sr_xCuO₄|STO,¹⁵ ferromagnetic LaCoO₃|LAO,¹⁶ and ferroelectric BaTiO₃|DyScO₃.¹⁷ Interfacial engineering has also made impactful contributions in the field of multiferroicity by transforming a “boring,” paraelectric and antiferromagnetic insulator such as EuTiO₃, into one of the strongest known multiferroics that has 100 times improved spontaneous polarization and magnetization over the next-best material.^{18,19} Materials interfacing is also finding strong grounds in the design of better

Contributing Editor: Edward M. Sabolsky

^{a)}Address all correspondence to this author.

e-mail: daidhy@uwyo.edu

^{b)}This author was an editor of this journal during the review and decision stage. For the *JMR* policy on review and publication of manuscripts authored by editors, please refer to <http://www.mrs.org/jmr-editor-manuscripts/>.

A previous error in this article has been corrected, see 10.1557/jmr.2016.15.

DOI: 10.1557/jmr.2015.327

radiation tolerant materials for nuclear applications,^{20–23} where these novel materials show higher sink strengths in the mitigation of irradiation-induced point defects, thus providing routes for preventing materials swelling. Besides these areas, design of interfacial materials is also being actively pursued in thermoelectricity,^{24,25} nanomechanics,²⁶ optoelectronics²⁷ and electrochemistry.^{11,28,29} All these examples highlight the importance and impact of interfaces in the future materials design.

In this review, with an overarching theme of microstructure design, we focus on the current understanding and the role of materials' interfaces in the design of materials for fast oxygen diffusion for electrochemical applications. Over the past two decades, the most important goal in the design of electrolytes has been to lower the solid oxide fuel cell (SOFC) operating temperatures to 500–700 °C, so as to use less expensive materials in interconnects and heat exchangers, and increase durability by reducing problems associated with thermal cycling.^{30,31} However, lower temperatures have a degrading effect on the kinetics of electrocatalytic reactions and the overall cell voltage. Thus, the research has been largely concentrated on unearthing materials that provide rapid oxygen diffusion at lower temperatures.^{32–38} In such a pursuit, with fluorite based materials such as yttria stabilized zirconia (YSZ) and ceria being long identified as the most likely candidates,^{39–41} the prime focus has been on dopant engineering to enhance bulk oxygen conductivity.^{42–46} Under this umbrella of work, critical concepts such as identifying the best dopant for the host cation, optimizing dopant concentration, vacancy ordering, elastic and electrostatic effects on vacancy–dopant association, double-doping strategies, etc. were developed.^{44,47–52} These experimental efforts supported by theoretical calculations indeed led to the development of some of the highest oxygen conducting materials, such as $\text{Dy}_{0.08}\text{W}_{0.04}\text{Bi}_{0.88}\text{O}_{1.56}$, $\text{Er}_{0.4}\text{Bi}_{1.6}\text{O}_3$ and $\text{Sm}_{0.075}\text{Nd}_{0.075}\text{Ce}_{0.85}\text{O}_{2-x}$.³⁰ Unfortunately, higher conductivity has come at the expense of lower thermodynamic stability of some of these materials, and efforts, such as using bilayered electrolytes, are being investigated to overcome these problems.³⁰ More recently, triggered by a seminal paper on $\text{BaF}_2|\text{CaF}_2$ superlattices¹ that showed a significantly large increase in ionic conductivity as a function of layer thickness, the field of electrolyte design has focused on microstructural features, and materials interfaces are currently at the forefront.⁵³

Interfaces, both hetero- (between two different materials), and homo- (e.g., grain boundaries and crystalline–amorphous interfaces) are being explored to understand oxygen vacancy diffusivity and the underlying mechanisms of transport. Figure 1 shows a broad overview of microstructural characteristics of both types of interfaces affecting oxygen vacancy dynamics and the resulting conductivity. In both types, fast oxygen transport is

expected to occur locally at the interfaces, as shown in Figs. 1(a) and 1(b). In heterointerfaces, such as in thin-films or multilayers, due to the lattice mismatch between the two adjoining materials, one of the materials is generally under tensile strain. This is increasingly becoming apparent that tensile strain could be used to lower oxygen vacancy migration barriers. A schematic of oxygen vacancy hopping in an unstrained and strained lattice, and the lowering of the barrier, is shown in Fig. 1(c). This concept for lowering migration barriers via interfacial strain is the leverage that is being explored in heterointerfacial materials. On the grain boundaries front, earlier work especially on metals showed that grain boundaries could act as channels for fast atomic diffusion due to the availability of open space. This *excess volume* at the grain boundaries [Fig. 1(d)] is expected to provide faster oxygen diffusion, and is the driving force for the interest in grain boundaries. Besides the effects of interfaces on the kinetics of oxygen vacancies, there is growing evidence that thermodynamics of oxygen vacancies could also be significantly manipulated by interfaces.^{54–56} Recent theoretical reports have predicted that vacancy concentration can be controlled via interfacial strain,^{57,58} where it has been shown that the formation energy of oxygen vacancies decreases under tensile strain leading to a higher concentration.^{58,59} One could thus imagine a strain-controlled oxygen vacancy concentration that could be tuned to the interfacial strain across the adjoining materials as shown in a schematic in Fig. 1(e). Such an increase in oxygen vacancy concentration coupled with lower migration barriers would be highly advantageous for oxygen transport. Segregation of oxygen vacancies to grain boundaries has also been well documented in oxide materials. The vacancy segregation profile of a grain boundary in CeO_2 is shown in Fig. 1(f). Thus, both heterointerfaces and grain boundaries could be used to control kinetics and thermodynamics of oxygen vacancies. The thermodynamic control would be even more useful as there is a growing appreciation for the critical role of oxygen vacancies^{54–56} in the physics of interface/thin-film structures based on transition-metal oxides for magnetic and electronic applications. There are also reports of high-temperature superconductivity induced by ordered oxygen vacancies.⁶⁰ In addition, the oxygen vacancies are found to act as healing agents in materials under radiation environments paving ways for the design of better radiation tolerant materials for nuclear applications and radioactive waste storage.^{61,62} Therefore, understanding of microstructure-influenced properties of oxygen vacancies is currently of much wider interest in the oxide community.

While interfaces provide exciting routes to novel materials design, understanding the interfacial structures and the associated energetics of oxygen vacancies is an extremely complex problem. For example, oxygen vacancy energetics at interfaces is guided by the inter-

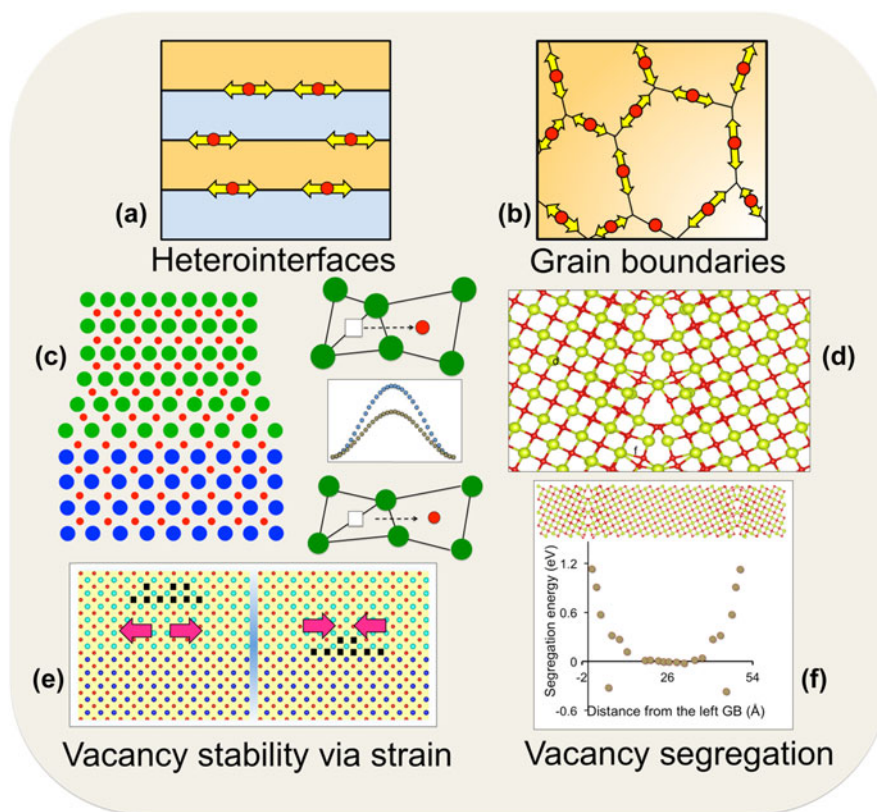


FIG. 1. Interfacial features for fast oxygen ion-diffusion at (a) layered heterointerfaces. (b) Grain boundaries. (c) Tensile strain on substrate material lowers oxygen migration barrier due to bond stretching. (d) Excess volume at grain boundaries. (e) Interfacial-strain controlled vacancy stability. (f) Vacancy segregation at grain boundaries.

twined effects of segregated dopant–vacancy interaction, interface–vacancy interaction, and dopant–interface interaction, all of which are simultaneously active, in contrast to only the dopant–vacancy interaction in the bulk. Similarly, the concentration of oxygen vacancies would not only be dictated by the initial dopant concentration; rather an additional effect of interfacial strain and atomic chemistry would also play a key role. Additionally, since some of the interfacial materials could experience strains as large as 5–7%, the materials may not remain in their thermodynamically stable phase as intended during synthesis; they could experience phase changes near the interfaces, or, could relax by forming misfit dislocations. All of these interrelated microstructural phenomenon would significantly affect oxygen conductivity. Thus, understanding these phenomena and their effects in isolation by disentangling them from each other is currently one of the most important challenges. In the following, we discuss the state-of-the-art understanding of some of these microstructural features and their effects on oxygen vacancy energetics.

II. INTERFACE EFFECTS ON OXYGEN DIFFUSION

While there has been some success in achieving higher oxygen diffusivity in both types of interfaces, results

from different researchers have been inconsistent, and at times even contradictory.^{6,63–65} There are groups of reports showing evidence of increase, decrease, or no change in oxygen conductivity at heterointerfaces compared to bulk. Among the various experiments carried out over the years, one of the most highlighted results is a stunning 8 orders of magnitude increase in oxygen conductivity reported in a YSZ|STO interface attributed to 7% tensile strain in YSZ.⁶ This is a standalone result that other research groups have failed to reproduce, and speculations regarding measurements of electronic rather than ionic conductivity have been made.⁶⁴ However, there are other mutually agreeable conductivity-increase reports where up to 3 orders magnitude increase has been reported. For example, Kosacki et al.⁶⁶ reported 1–2 orders of magnitude increase in YSZ (001) films deposited on MgO (001) substrates for films of 15 nm thickness. Sillassen et al.⁶⁷ reported about 3 orders of magnitude increase in YSZ films grown on, MgO (110), MgO (111) and STO different substrates. Karthikeyan et al.,⁶⁸ and Jiang et al.⁶⁹ also observed similar conductivity increases in YSZ grown on MgO, Al₂O₃, and Si substrates. Conductivity increases of similar magnitudes were also observed in gadolinium doped ceria (GDC) by Suzuki et al.⁷⁰ and Huang et al.⁷¹ Multilayered structures studied by Korte, Janek and co-workers^{72–75} have also

shown such conductivity increases and also illustrated a consistent strain–conductivity relationship by considering multilayers of YSZ, under compressive, tensile or no strain conditions, interfacing with Sc_2O_3 , Lu_2O_3 or Y_2O_3 , respectively. They demonstrated that oxygen diffusivity is directly related to the applied strain, i.e., it increases under tensile strain and decreases under compressive strain. In contrast, other research groups have reported conductivity decreases even though YSZ was grown on similar substrates. For example, Guo et al.⁷⁶ deposited YSZ on MgO (100) and Navickas et al.⁷⁷ deposited YSZ on Si (001). Both these studies reported 3–4 times decrease in conductivity compared to polycrystalline YSZ. Jung et al.,⁷⁸ Gerstl et al.,⁷⁹ and Pergolesi et al.,⁶³ reported no observable change in ionic conductivity of YSZ films grown on similar substrates, as discussed above.

On the grain boundaries front, while it is generally perceived that grain boundaries have blocking effects on oxygen vacancy diffusivity, there is significant evidence of conductivity increase, and thus the oxygen conductivity results on grain boundaries have also remained controversial. Knoner et al.,⁶⁵ presented the first measurements of oxygen grain boundary diffusion in nanocrystalline YSZ, and reported 3 orders of magnitude increase in conductivity compared to single crystals. Later Bellino et al.⁸⁰ reported an order of magnitude increase of conductivity in nanocrystalline yttria doped ceria (YDC) and samarium doped ceria (SmDC) compared to microcrystalline samples. An et al.⁸¹ have recently reported 4 orders of magnitude decrease with increasing grain size in nanocrystalline YDC. In contrast, Lee et al.⁸² and Maglia et al.⁸³ reported no change in oxygen conductivity in nanocrystalline GDC and SmDC, respectively. Similarly, De Souza et al.⁸⁴ reported no change to a minor decrease in nanocrystalline YSZ. Souza et al.⁸⁵ reported a monotonic decrease with decrease in grain size in nanocrystalline SmDC, and Guo⁶⁴ also reported a conductivity decrease with decreasing grain size in nanocrystalline YSZ. Thus, similar to hetero-interfaces, there is a wide diversity of results on grain boundaries, and there is no real qualitative agreement.

These contrasting results showcase not only the limited understanding of oxygen energetics at interfaces but also illustrate the diverse outcomes that could possibly originate due to material synthesis. Jiang et al.⁸⁶ highlighted the comparison between oxygen conductivity values between bulk and interfaces in the literature. They pointed out that while there is relatively good repeatability among the bulk samples, despite different preparation methods, dopant contents and purity, as evidenced by a narrow activation energy range between 1.02 and 1.24 eV, that the range for interfaces widens to 0.62–1.24 eV. These differences allude to the underlying fact that, even though there is an ever-increasing control

over materials' growth, synthesis conditions, including temperature, oxygen partial pressure and annealing rates, could still have a significant effect on the nanometric level microstructure features that dictate oxygen energetics at interfaces.

A. Dopant segregation

Over the years, one microstructural process that has been consistently referred to be associated with materials' synthesis is impurity/dopant segregation. It is a widely observed phenomenon and has been believed to be partly responsible for limiting oxygen conductivity.

1. Dopant segregation at grain boundaries

Using high resolution transmission electron microscopy and scanning transmission electron microscopy (STEM), Li et al.,⁸⁷ recently showed direct evidence of Gd segregation in nanocrystalline GDC, and their results revealed that dopants can not only form defective clusters inside the bulk, but also can form at the grain boundaries. Previously, de Ridder et al.⁸⁸ showed dopant (Si, Ca and Na) segregation on the surface of YSZ leading to reduction in electrocatalytic activity at the surface. Similarly, using a Z-contrast imaging in combination with electron energy loss spectroscopy (EELS), Lei et al.⁸⁹ showed Y segregation at a bicrystal tilt grain boundary in YSZ. Aoki et al.⁹⁰ also reported Ca and Si segregation in CaO-stabilized ZrO_2 . Dopant segregation has also been quite widely studied computationally from atomistic simulations. Both density functional theory (DFT) calculations and atomistic calculations have predicted dopant segregation in a variety of oxide materials, and both elastic and electrostatics effects leading to segregation have been studied. For instance, Lee et al.⁹¹ performed kinetic Monte Carlo simulations on YSZ and GDC and showed that the dopant concentration increased near the surfaces. Yoshiya and Oyama⁹² studied a variety of tilt grain boundaries in YSZ and showed that Y segregation is largely associated with oxygen vacancies at the grain boundaries, although the

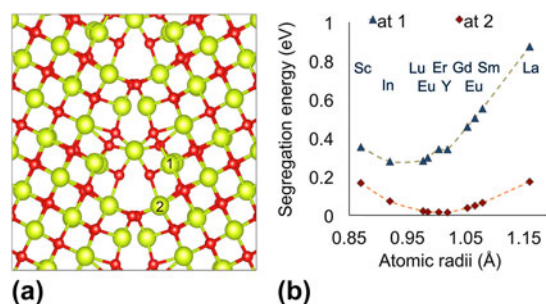


FIG. 2. Dopant segregation at grain boundaries. (a) $\Sigma 5$ (310) (001) tilt grain boundary in CeO_2 . (b) Segregation energy for two cation sites at the boundary.

segregation energy varied among different grain boundaries. Figures 2(a) and 2(b) are representatives of typical computational calculations generally shown in the literature. Figure 2(a) shows a schematic of the $\Sigma 5$ (310) $\langle 001 \rangle$ tilt grain boundary in CeO_2 , and Fig. 2(b) shows the dopant segregation energy for a variety of +3 lanthanides calculated using static pair-potentials via the Large-scale atomic/molecular massively parallel simulator (LAMMPS) code⁹³ for two cation sites, as shown in Fig. 2(a). The positive segregation energy indicates that dopants prefer to segregate at the grain boundary. In addition, the data show that the segregation energy is related to dopant radii, i.e., there is a minimum in the segregation energy for the dopants that have similar radii to the host cation.^{94,95} Dopant segregation has also been purposefully used in preventing grain growth in oxide materials. Chen and Chen⁹⁶ showed that not only grain boundary diffusion could be prevented by adding lanthanide dopants, but the rate of grain growth could also be varied based on the dopant type. Such dopant-influenced grain growth was recently captured by molecular dynamics (MD) simulations, and it was shown that the dopant radius affects grain boundary mobility by controlling oxygen vacancies at the grain boundaries.⁹⁷

2. Dopant segregation at heterointerfaces

Apart from grain boundary segregation, dopant segregation has also been observed in heterointerfaces. A transmission electron microscopy interfacial study by Simon et al.⁹⁸ on the heterointerfacial structures between $\text{La}_{2/3}(\text{Ca}/\text{Ba})_{1/3}\text{MnO}_3/\text{STO}$ revealed that there is a preference for Ca cation segregation to the interfaces. Estrade et al.⁹⁹ captured the interfacial strain induced dopant segregation in $\text{La}_{2/3}\text{Ca}_{1/3}\text{MnO}_3$ (LCMO) by depositing on (001) and (110) SrTiO_3 substrates. They observed that while the (110)-deposited relaxed films showed homogeneous distribution of La and Ca, the unrelaxed (or strained) (001)-deposited films showed a composition gradient, i.e., tensile strain induced La segregation at the

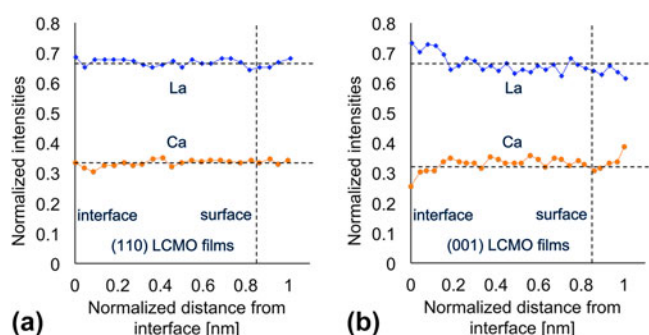


FIG. 3. Ca and La weighted intensities in LCMO/STO interface structure as a function of normalized distance from the interface. (a) For (110) deposited LCMO films, (b) for (001) deposition LCMO films. The horizontal lines indicate initial composition, and the vertical line indicates a distance of 3.5 nm below the surface. Reproduced from Ref. 99.

interfaces, whereas Ca segregated to the surfaces. This observation is shown in Fig. 3 where Fig. 3(a) shows a homogeneous distribution of both La and Ca across the (110)-deposited film (i.e., both at the interface, inside the film, and at the surface), whereas Fig. 3(b) shows a gradient-distribution of La and Ca in (001)-deposited film, thus indicating strain-induced cation segregation. However, such studies on cation-segregation at heterointerfaces are limited compared to those in grain boundaries, and the effects of interfacial strain on dopant segregation are not well understood. Figures 4(a) and 4(b) represent strain-influenced dopant segregation in a heterointerfacial structure. Here, dopant segregation is calculated in CeO_2 which is interfaced with ZrO_2 or ThO_2 . The purpose of these two interfacing materials is to introduce different directional strains in CeO_2 , i.e. interfacing with ZrO_2 introduces compressive strain in CeO_2 due to its larger lattice parameter than ZrO_2 , whereas interfacing with ThO_2 introduces tensile strain due to its smaller lattice parameter than ThO_2 . A distinctive model structure, as shown in Fig. 4(a) is used for these calculations so as to introduce the gradient effect of interfacial strain on interatomic distances. As Fig. 4(a) shows, while in the interior of either of the materials, the oxygen–oxygen distances are closer to their bulk distances, i.e., O–O distance of 2.59 Å in ZrO_2 is closer to 2.55 Å in ZrO_2 -bulk, and 2.68 Å in CeO_2 is closer to 2.70 Å in CeO_2 -bulk; however at the interface, the O–O distance is an average of the two materials, i.e., 2.64 Å. (O–O distance trends in CeO_2 - ThO_2 would be opposite; they are not shown here.) Using this structure, the segregation energy is calculated by placing a dopant at the interface and comparing to the one in the center of CeO_2 . Figure 4(b) shows the trends of segregation energy for the two systems, as a function of +3 lanthanide dopant radii. The positive segregation energy represents preference for segregation. Segregation energies for CeO_2 - ZrO_2 structure are shown in green circles; whereas, those for CeO_2 - ThO_2 are shown in orange diamonds. We find that the trends are opposite for

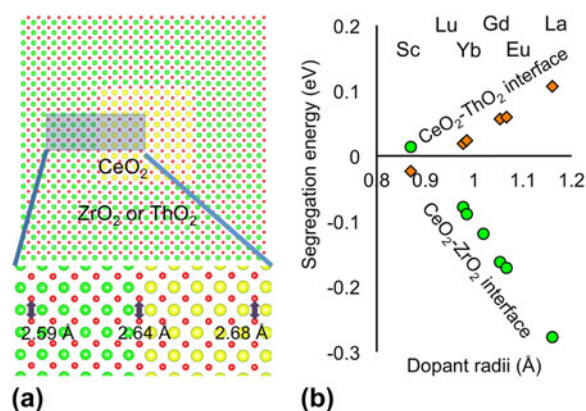


FIG. 4. Dopant segregation at heterointerfaces. (a) Model heterointerface structure showing between $\text{ZrO}_2/\text{CeO}_2$ showing the change in O–O distance due to interfacial strain. (b) Dopant segregation in CeO_2 - ZrO_2 and CeO_2 - ThO_2 interfaces.

the two systems, i.e., most of the dopants prefer to segregate at the interface in the $\text{CeO}_2\text{-ThO}_2$ structure, whereas they prefer to stay inside the CeO_2 bulk in the $\text{CeO}_2\text{-ZrO}_2$ structure. This opposite behavior can be primarily attributed to the opposite directions of the interfacial strains, i.e., tensile strain introduced by ThO_2 allows larger free volume at the interface, and the dopants that are larger in radii than Ce are easily accommodated at the interface. Conversely, the compressive strain introduced by ZrO_2 provides smaller free volume at the $\text{ZrO}_2\text{-CeO}_2$ interface than that the dopants experience inside CeO_2 ; as a result larger dopants prefer to stay inside CeO_2 bulk. The only dopant, Sc, that is smaller than Ce shows an opposite trend relative to the rest of the dopants, as expected.

3. Effect of dopant segregation on oxygen energetics

While grain boundaries are generally viewed as blocking agents against oxygen conductivity, it is likely that dopant segregation could be the actual culprit. Very recently, An et al.⁸¹ performed experiments comparing the oxygen conductivity in the as-grown and annealed YSZ samples. They observed that the ionic conductivity decreased with the annealing time as the grain size grew from 10 to 50 nm at 1200 °C after 10 h. The Arrhenius plot of the as-deposited, 1000 °C annealed and 1200 °C annealed samples is shown in Fig. 5. The authors pointed out that even though the as-deposited samples had smaller grains (i.e., higher grain boundary density), the ionic conductivity was comparable to that of the microcrystalline samples that had much lower grain boundary density, as shown in Fig. 5. The grain boundary conductivity of the as-deposited samples decreased up to 2 orders of magnitude upon annealing at 1200 °C even though grain growth

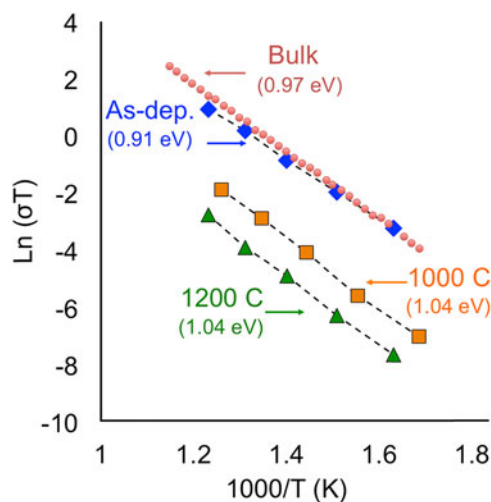


FIG. 5. Arrhenius plot of as-deposited, 1000 °C annealed and 1200 °C annealed 12 mol% YDC samples. Oxygen conductivity decreases as grain size increases due to grain growth under high temperature annealing. Reproduced from Ref. 81.

occurred during annealing. Similar trends were reported by Tian and Chan¹⁰⁰ where they observed higher oxygen conductivity in fine-grained YDC compared to larger-grained YDC. They observed that samples sintered at 1400 °C showed higher oxygen conductivity than those sintered at 1500 °C, and argued that larger density of grain boundaries in 1400 °C samples provided more area for the dopants to segregate for a given concentration of dopants. Eventually dopant segregation could cause depletion in the oxygen vacancy concentration in the vicinity of the grain boundaries as per the space-charge layer model,^{101,102} thus reducing the overall conductivity. Thus, in view of these experimental observations, it appears that instead of the blocking effect of grain boundaries, larger focus may be required on preventing dopant segregation.^{81,94}

Theoretical calculations on oxygen energetics at grain boundaries and heterointerfaces illustrate the effect of dopant segregation on oxygen vacancy migration and binding energies.⁹⁴ The inset in Fig. 6(a) shows a grain boundary structure with two oxygen migration locations, i.e., one in bulk and the other almost at the grain boundary. Migration barriers for paths parallel (shown by dots) and

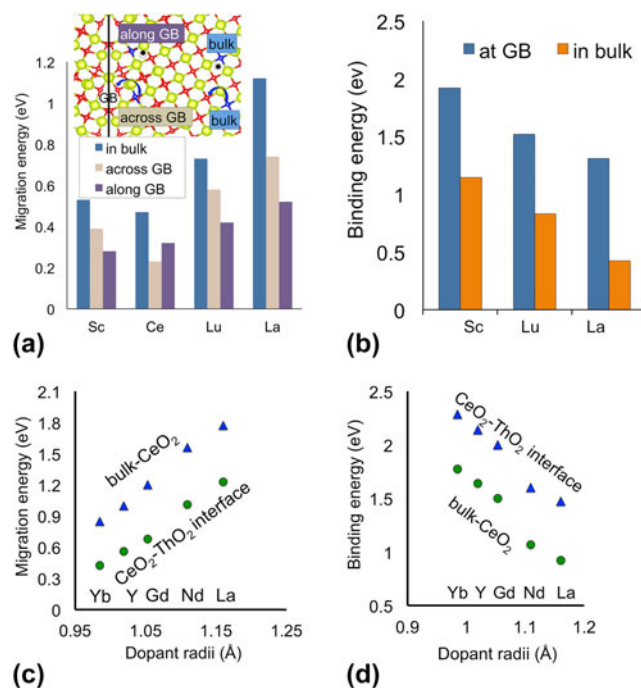


FIG. 6. Oxygen energetics at grain boundaries and heterointerfaces. (a) Oxygen vacancy migration energy in bulk and near grain boundary in undoped and doped CeO_2 both along and across the grain boundary. The migration energy decreases near grain boundaries. (b) Comparison between dopant-oxygen vacancy binding energy at grain boundary and in bulk. The binding energy is higher at grain boundaries than in the bulk. (c) Comparison between oxygen vacancy migration energies at the $\text{CeO}_2\text{-ThO}_2$ interface to that in the bulk- CeO_2 in the presence of dopants. The migration energies are lower at interfaces than in bulk- CeO_2 due to tensile strain at the interface. (d) Dopant-oxygen vacancy binding energy at the interface and in the bulk. The binding energies are lower in the bulk compared to that at the interface.

perpendicular (shown by curved arrows) to the grain boundary are calculated. A dopant is placed as a nearest neighbor in the vicinity of the diffusing oxygen vacancy to calculate its effect on the migration barrier. Three dopants are considered, i.e., Sc^{3+} , Lu^{3+} and La^{3+} that have 0.87, 0.977 and 1.16 Å ionic radii, respectively, compared to that of 0.97 Å of Ce^{4+} host cation. First, in the undoped case (labeled Ce), migration barriers decrease near the grain boundary irrespective of the direction of diffusion. Second, the trend remains same even in the presence of the dopants. This shows that, for systems with the similar dopant type, oxygen diffusivity should always be higher at the grain boundaries compared to that in the bulk. Thus, it appears that the blocking effect of grain boundaries may not originate simply from migration barriers.

The reduction in oxygen conductivity at the grain boundary may actually originate from the dopant–vacancy binding energy. Figure 6(b) shows the binding energies between the dopant and oxygen vacancy inside the bulk and near the grain boundary. First, it is found that the binding energy decreases as the dopant size increases, in agreement with the previous literature. Second, it is found that the binding energy at the grain boundary is much higher compared to that in the bulk. For instance, the binding energy for Sc inside the bulk is 1.19 eV but it is 1.92 eV at the grain boundary, thus increasing by almost a factor of 2.⁹⁴ Such a high increase in the binding energy could actually be the major reason behind reduced oxygen conductivity at the grain boundaries. While the result presented here are for a dimer complex consisting of one dopant and one vacancy pair, similar trends are observed for trimer complexes consisting of two dopants and one oxygen vacancy.⁹⁴

Similar observations are made in the heterointerface systems. Using the same $\text{ThO}_2\text{--CeO}_2$ heterointerface system as above, the migration and binding energies are plotted in Figs. 6(c) and 6(d), respectively. Previously, from DFT calculations on bulk systems, it was shown that migration barriers could be decreased by applying tensile strain.¹⁰³ Here, the barriers are calculated at the strained heterointerface with dopants present as nearest neighbors of diffusing oxygen vacancies. Figure 6(c) shows that for all dopants, the migration barriers are lower at the interface than that in the bulk. This is due to the tensile strain experienced by CeO_2 at the interface. Thus, these simulations provide evidence on the lowering of oxygen migration barriers at heterointerfaces under tensile strain. Figure 6(d) shows the comparison of binding energies between the interfaces and bulk. It is again found that the binding energy is significantly higher at the interface. Thus, based on these calculations, a common theme emerges that both grain boundaries and heterointerfaces could provide low migration barriers sites for oxygen diffusion. However, segregation of dopants could lead to higher binding energies that may prevent oxygen vacancies from participating freely in conduction. These theo-

retical results thus seem to agree with the recent experimental observations by An et al.,⁸¹ i.e., dopant segregation has a more pronounced impact on oxygen conductivity than grain boundary density. Therefore, to take leverage of microstructural properties, preventing dopant segregation may need to be kept in prime focus in the design of fast oxygen conducting materials.

III. COUPLING BETWEEN HETEROINTERFACES AND POINT DEFECT CONCENTRATION

Oxide heterointerfacial materials are increasingly becoming potential candidate materials for next-generation electronic devices. These materials possess extremely diverse and groundbreaking properties such as high T_c superconductivity, colossal magnetoresistance, multiferroic behavior, giant photoconductivity, resistive switching, photoelectrochemical water splitting, and giant thermoelectricity.^{104–106} Interfacing two different materials breaks translational and rotational symmetry, introduces strain and space charge, and creates new atomic bonds. Such modifications often lead to the formation of oxygen vacancies, which are the most common point defects in oxide materials. These interface/strain induced oxygen vacancies have opened up a vast new field of research, and while the understanding is still superficial, oxygen vacancies are increasingly pointed out to be responsible for variety of the novel properties.^{8,107–110} Thus, there is unrest in the community to understand the coupling between interfacial strain and oxygen vacancy stability making it a crucial topic of interest.

A. Strain-effected oxygen vacancy formation energy in bulk

While a combination of various microscopy techniques, such as high-angle annular dark-field (HAADF), STEM and EELS, are being used to probe oxygen vacancies,^{54,108} theoretical calculations are at equal footing in complementing them by revealing the vacancy formation energetics in the interfacial structures. In particular, DFT calculations have been recently used to understand the effect of strain on oxygen vacancy formation energies. Figure 7(a) shows the formation energy as a function of strain in bulk CaMnO_3 .⁵⁹ The formation energy decreases with strain, indicating that higher oxygen concentration could be expected in heterostructures consisting of CaMnO_3 under tensile strain. A partly similar observation is made in Fig. 7(b) shows the vacancy formation energy in CeO_2 .⁵⁸ Again, the formation energy decreases with increasing tensile strain. Its behavior under compressive strain is however different from that of CaMnO_3 , i.e., while the vacancies in CaMnO_3 seem to be unresponsive to compressive strain, their formation energy increases in CeO_2 . The data in Fig. 7(a) further show that the two crystallographically

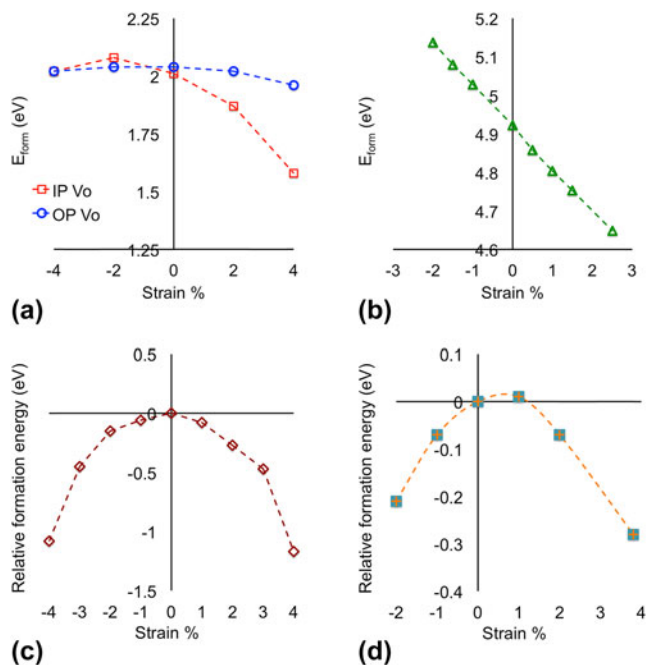


FIG. 7. Oxygen vacancy formation energies under tensile strain for (a) CaMnO₃ and (b) CeO₂. Relative oxygen vacancy formation energy with respect to no strain in (c) SrTiO₃ and (d) La_{0.5}Sr_{0.5}CoO_{3- δ} . The data in (a), (c) and (d) are reproduced from Refs. 59, 109, and 110, respectively.

different oxygen sites have different responses to the applied strain. Similar observations were recently made in the pyrochlore structure, such as La₂Ti₂O₇, where the two crystallographically different vacancies were predicted to have different chemical expansions under strain.¹¹¹ These varying responses are not very well understood yet, however, they open a possibility of another degree of freedom in functionalizing the vacancies. Nevertheless, these results show that there is a strong strain–vacancy coupling, and it could be material dependent.

This material dependence is further highlighted by the trend in the formation energy in STO. Using DFT calculations, Choi et al.,¹¹² calculated the vacancy formation energy in STO. Interestingly, they observed that the formation energy decreased irrespective of the direction of strain [Figs. 7(c)], i.e., both compressive and tensile strains reduced the formation energy. While the decrease in formation energy under tensile strains could be understood from the chemical expansion concept, where it is generally perceived that oxygen vacancies occupy larger lattice volume compared to the oxygen ion, and thus stabilizing the vacancy in a larger volume provided by tensile strain. The observation of its decrease under compressive strain is interesting. Choi et al. postulated such response to a decrease in the band gap in STO, which they found to occur under both compressive and tensile strains. This observation in STO is not unique, as Donner et al.¹¹³ also found the same behavior

in La_{0.5}Sr_{0.5}CoO_{3- δ} as shown in Fig. 7(d). These different observations not only unveil the limited understanding of oxygen energetics under strain, but also display how complex such behavior could be. However, as an upshot, they open up myriad possibilities to unravel even more interesting interfacial properties.

B. Strain-controlled oxygen vacancy concentration across heterointerfaces

Calculating bulk formation energies provides a general idea on oxygen energetics in a given material. However, in the interface structure, formation/stability of oxygen vacancies would not only depend on the bulk formation energy, but other factors, including interfacial strain, atomic chemistry and chemical gradient, could play a significant role. Thus, there could possibly be a competition between the two materials on either side of the interface, and the situation could be more complex. Since this field is still emerging, there is only a handful of evidence of such strain-influenced vacancy stability interface calculations.^{57,58,114,115} DFT calculations were recently performed on a (001) STO|(001) MgO model interface structure to explore the stability of oxygen vacancy across the interface structure.⁵⁷

Figure 8(a) shows the TiO₂-terminated STO|MgO interface structure. Four locations for the oxygen vacancy, i.e., inside STO (A), at the interface in STO (B), at the interface in MgO (C) and inside MgO (D) were tested. The structure was strained at the interfacial plane using lattice parameters of STO (3.94 Å), MgO (4.24 Å) and multilayer (4.03 Å). These are labeled as (1), (2) and (3), respectively, in the legend of Fig. 8(b). Thus, by using the lattice parameter of STO, MgO comes under compressive strain due to the smaller STO lattice parameter; in (2), STO comes under tensile strain due to the larger MgO lattice parameter; whereas in (3) the strain corresponds to 4.03 Å, which is an average lattice parameter between STO and MgO. It is to be noted that such high strains may at times be unrealistic, and are largely used here to theoretically elucidate their effects on oxygen vacancies. Figure 8(b) shows the stability at four vacancy locations for all three strain cases plotted with reference to site A. The vacancy is stable deep inside STO for strain cases (2) and (3), and is stable at the STO-side of the interface for strain case (1). These results indicate that the oxygen vacancy prefers to stabilize in the tensile-strained STO material and does not prefer compressively-strained MgO. When the interface is strained even further such that MgO is also tensile-strained, the stability starts to decrease, as shown in Fig. 8(c) by the “V” shaped plot. This behavior may possibly indicate that beyond a certain tensile strain, MgO gets tensile-strained enough to start providing stability to the vacancy. For the strain data

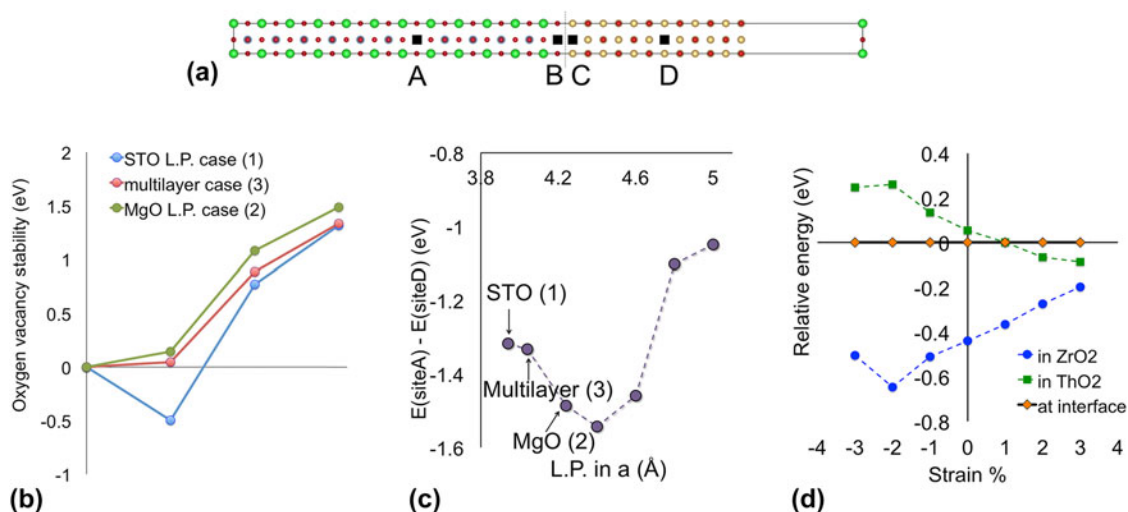


FIG. 8. Oxygen vacancy stability in the $\text{SrTiO}_3|\text{MgO}$ interface in (a)–(c). (a) Interface structure and four locations tested of oxygen vacancies tested for stability represented with black squares. (b) Comparison of oxygen vacancy stability at four locations with reference to site A. Calculations are done for the three strain cases as discussed in text. (c) Oxygen vacancy stability difference between site A and D under increasing strain. (d) Oxygen vacancy relative stability in the $\text{ZrO}_2\text{--ThO}_2$ interface with reference to vacancy stability at the interface (orange diamonds).

presented, the stability does not flip in the favor of MgO ; however, such a possibility can indeed exist.

Similar DFT calculations on a model interface between fluorite based ThO_2 and ZrO_2 showed that oxygen vacancies could be preferably stabilized across the interface as a function of interfacial strain.⁵⁸ Figure 8(d) shows the oxygen vacancy stability between the $\text{ThO}_2|\text{ZrO}_2$ interface at three locations, i.e., inside bulk- ZrO_2 , at the interface and inside bulk- ThO_2 plotted with reference to its stability at the interface. The details on the interface structure can be found elsewhere.⁵⁸ Since ThO_2 has a larger lattice parameter than ZrO_2 , it is under compressive strain; whereas ZrO_2 is under tensile strain. For all of the data points, the oxygen vacancy is stable inside ZrO_2 compared to ThO_2 and the interface. The more interesting comparison, however, is between ThO_2 and the interface. At zero strain, the vacancy is stable at the interface, but as strain increases, its stability begins to change, and by 2% strain, the vacancy now stabilizes inside ThO_2 . From the data trend, it can be predicted that beyond 3% strain, ThO_2 could become the most stabilizing location among all the three cases. Thus, these calculations show that oxygen vacancy stability is largely dependent on the strain experienced by interfacing materials. Calculations on the $\text{ZrO}_2|\text{CeO}_2$ interface were also performed recently^{114,115}; while these calculations did not include any external strain, and the materials were simply allowed to relax to the average strain. As a result, ZrO_2 was under tensile strain and CeO_2 under compressive. These calculations showed that vacancies preferred to segregate at the interface. It is quite clear that such studies are at initial stages, and more calculations on other systems are warranted for profound understanding

of oxygen energetics at interfaces. It is also evident that calculating the formation energies in bulk materials may provide only a partial picture of oxygen vacancy stability. Instead, for strain to act as a controlling “knob” to preferably stabilize oxygen vacancies on either side of the interface, interfacial chemistry and chemical gradients play a key role, and calculations on actual heterointerface structures would make a larger impact. Control over the interfacial strain and the resultant vacancy stability promises opening up of wide opportunities for designing heterointerface materials.

IV. NEAR-INTERFACE PHASE TRANSITION

Oxide materials can accommodate significant amount of strain at interfaces, and modern physical deposition techniques can grow thin films with great control at the atomic level. Particularly, layer-by-layer growth of perovskite materials has become a routine task, and the microscopic characterization can clearly reveal columns of cations and oxygen atoms. Identification of termination planes, misfit dislocations and atomic interdiffusion is at early stages, although there are few studies that have microscopically captured such changes. Strain-induced phase transition at interfaces is an interesting phenomenon that has gathered interest, particularly in the $\text{YSZ}|\text{STO}$ interface. At this interface, YSZ undergoes 7% tensile strain due to the lattice mismatch with STO , and was reasoned for the very high oxygen conductivity at the interface.^{6,116–118} Using DFT calculations and a combination of STEM and EELS, it was suggested that the high conductivity originated due to the disordered YSZ oxygen sublattice.¹¹⁷ It was shown that clear columns

of oxygen atoms could be identified in the adjoining STO, while those in YSZ were blurred, providing evidence of the disorder. A possibility of strain-induced phase transition had been speculated.

Theoretical calculations have since been performed to understand this near-interface phase transition. Using a combination of DFT and atomistic calculations, Cheah and Finnis¹¹⁹ mapped out the various possible phases that could be stable under tensile strain. Using energy versus strain plots, in a fair agreement between the two simulation methods, they showed that with the increase in tensile strain, the fluorite phase could transform to columbite and anatase phases at 4 and 8% tensile strains, respectively. Recently, DFT calculations were performed on model $\text{ZrO}_2|\text{CeO}_2$ and $\text{ZrO}_2|\text{ThO}_2$ interfaces.⁵⁸ In both cases, it was found that, since ZrO_2 has a smaller lattice parameter than the other two materials, the interfacial tensile strain transformed the fluorite phase into the columbite phase. More recently, Tarancón and Morata¹²⁰ performed MD simulations of strained YSZ and found that both cation and oxygen sublattices undergo significant distortion at 4% tensile strains, possibly also indicating a phase transition. However, they did not identify the new phase. A similar strain-induced phase transformation has been previously observed in fluorite-based nanocrystalline UO_2 providing some support to these recent observations.¹²¹ On a broader view, the strain-induced phase transformations could be also expected in other materials, and future investigations are required to understand such structure–property relationships, and their effect on oxygen diffusion near interfaces.

Another example of near-interface phase transformation is in irradiated pyrochlore materials. In $\text{Gd}_2\text{Ti}_2\text{O}_7$, it has been found that swift heavy ion irradiation amorphizes the material and creates a circular amorphous ion track of a few nanometers in diameter.^{122,123} The interesting phase transformation occurs in the peripheral ring region of the track where the pyrochlore structure transforms to the defective-fluorite structure. The difference between these two structures is that while both the cations and the vacant oxygen site in pyrochlore are fully ordered, they are completely disordered in the defective-fluorite structure. Recent HAADF imaging of the ion tracks shows that the defective fluorite ring region could actually be under tensile strain.¹²⁴ Within 1 nm peripheral range of the track, tensile strain increased as the pyrochlore structure changed to defective fluorite. Concomitant DFT calculations support these observations by revealing that tensile strain could indeed stabilize the defective fluorite structure over the pyrochlore structure. A similar tensile strain as a function of phase transition is also observed in the supporting swift heavy-ion MD simulations.¹²⁴ Since pyrochlore materials contain one vacancy oxygen site per unit cell, these materials have been considered as possible fast ion conductors.

However, they have been limited by the ordered arrangement of ions. Previous theoretical simulations have shown that breaking the ordered arrangement unleashes the fast ion conducting property in the defective fluorite structure.¹²⁵ Unraveling of tensile-strain induced phase transformation now opens up the possibility to use the ring-regions of the irradiated materials as fast-ion channels, and also grows thin-films of tensile-strained pyrochlore materials as defective fluorites and possibly gain advantage of fast-ion conduction. In addition, oxygen vacancy migration barriers that can be simultaneously lowered via tensile strain would result in a two-pronged control over oxygen diffusion. Furthermore, trivalent dopants added to fluorite materials, which often segregate to interfaces and reduce oxygen conductivity by forming complex-defect associates are absent in pyrochlore materials. The free availability of oxygen vacancies in the defective-fluorite structure could be an additional factor in advancing the strain-engineered pyrochlore materials. Thus, near-interface phase transitions are interesting branched-out areas of interfacial materials that need to be studied both from the structure and properties point of view.

V. MISFIT DISLOCATIONS

Conventionally, misfit dislocations have been considered as fast atomic diffusion routes due to the presence of large open spaces. Such fast diffusion has been widely observed in metals, and pipe diffusion is the common term used to refer to fast diffusion via dislocations. At oxide heterointerfaces, recent microscopic studies have also captured misfit dislocations. Kalabukhov et al.¹²⁶ observed such dislocations at the LAO|STO interface interspaced at every 15 nm. Similarly, Zhu et al.¹²⁷ observed misfit dislocations at an interspacing of 13 nm in STO|MgO interfaces. There are many other reports of their observance at interfaces, such as in $\text{BaTiO}_3|\text{Sm}_2\text{O}_3$,¹²⁸ $\text{ZnO}|\text{Al}_2\text{O}_3$,^{118,129} and $\text{Pr}_{0.48}\text{Ca}_{0.52}\text{MnO}_3|\text{STO}$.¹³⁰ Since a high density of misfit dislocations is observed at oxide interfaces, they are another microstructural features that are being considered as possible fast-ion conduction pathways. Earlier experimental studies, such as those by Sillassen et al.⁶⁷ have attributed high ionic conductivity partly to misfit dislocations. However, there are no direct oxygen conductivity experimental measurements confirming such a possibility. Atomistic simulations have been conducted in this regard that have provided some indication of oxygen energetics. Marrocchelli et al.¹³¹ and Metlenko et al.¹³² conducted simulations on edge dislocation and 6° [001] tilt grain boundary in a STO bicrystal, respectively. In both studies, a common conclusion was reached that dislocations did not provide fast diffusion routes for oxygen conduction, and the results were in contradiction to what is observed in metals. Marrocchelli et al. showed that dislocations act as deep segregation spots for oxygen

vacancies, and the oxygen vacancy formation energy is 2.0 eV lower than that in the bulk, indicating a strong driving force for the vacancy to reside at the interface. They further showed that migration barriers are also significantly high, i.e., almost 2.0 eV compared to only 0.9 eV at dislocation sites. They concluded that although a high diffusion coefficient was observed at dislocations, the contribution largely originated from the high concentration of oxygen vacancy present at the dislocation core and not from the migration barrier that was found to be very high.

Using hybrid Monte Carlo and MD simulations, Sun et al.¹³³ also made similar observations on an edge dislocation in doped and pure CeO₂. They found that segregated dopants at the dislocation act as strong blocks to free movement of oxygen vacancies, and the dopant–vacancy interaction prevails. In the absence of dopants, they found that while tensile strain around the dislocation provided some enhancement in oxygen diffusivity, the compressive strain on the other side of the dislocation largely nullified it. Thus, no significant increase in oxygen conductivity was observed at dislocations.

In contrast to the above results, Murphy et al.¹³⁴ did observe a signature of pipe diffusion in UO₂. They performed diffusivity measurements using MD simulations on four dislocations, i.e., [100]{110}, [110]{110}, [101]{110} and a screw dislocation. Surprisingly, in all four dislocations, they observed enhancement in oxygen diffusivity, and the activation energies were significantly lower than those in the bulk. While these are interesting observations in contrast to others, Sun et al.¹³³ pointed out that the high diffusivity observed in UO₂ could be largely due to the interstitial oxygen diffusion, in contrast to the vacancy diffusion considered in their study. While these studies have opened up this area of research particularly in setting up the methodologies to perform such simulations, at this point, it is quite obvious that there simply aren't enough studies to fully elucidate dislocation effect on oxygen diffusion, and conclusions from these few results should be drawn with care. The understanding is still at an early stage, and it should not be surprising if the results could again turn out to be equally polarizing as the community experienced at grain boundaries and heterointerfaces.

VI. CONCLUSION AND OUTLOOK

From a decade of research on oxygen kinetics at interfaces, it appears that the field is starting to converge on some issues, at least on heterointerfaces. It is quite clear that synthesis methods still dictate the outcome of oxygen conductivity; however, recent theoretical calculations have at least established that oxygen migration barriers can be reduced by tensile strain. Epitaxial growth of thin films

should be able to take leverage of tensile strain in enhancing oxygen conductivity; presence of grain boundaries in thin films, however, appears to reduce the positive effect of tensile strain. On the grain boundaries front, whether they act as fast channels still seems to be under debate. High concentration of oxygen vacancies at grain boundaries under the space charge layer model is well established, and the segregation of dopants at grain boundaries is also widely captured. The binding between dopants and oxygen vacancies in forming defective clusters could actually be an important parameter that may decide the ultimate fate of oxygen conductivity. Recent experimental work such as by An et al.⁸¹ on understanding the coupling between dopant segregation—vacancy diffusion seems to be important and should be aggressively pursued in future. As the grain size decreases, the concentration of dopants segregated at grain boundaries increases. The high dopant–vacancy binding energy would prevent taking leverage of the open spaces at grain boundaries, thus impeding the transport. Doping strategies (i.e., choice of dopants) previously designed for microcrystalline materials that were primary targeted toward bulk may not be relevant in nanocrystalline materials. Rather novel strategies that prevent dopant segregation need to take prime focus.^{94,135} In the doped heterostructures, thickness of layers may also need to be optimized so as to induce maximum tensile strain while simultaneously reducing the large dopant concentration at interfaces. There are some studies that have indicated a layer-thickness dependence peak in oxygen conductivity, showing that maximum conductivity does not necessarily occur in the thinnest structures.¹³⁶ While the underlying reasons for such optimum thickness are not fully clear, dopant segregation could be playing a key role. Other recent strategies, such as free standing buckled membranes that have been recently shown to decrease oxygen migration barriers, are promising engineering methods to gain control over oxygen conductivity.¹³⁷

Gaining control over the oxygen vacancy concentration and distribution is also important for the overall design of layered oxide materials. Such strain-controlled thermodynamics coupled with kinetics of oxygen vacancies would be particularly beneficial for fast ion conductors, as both activation and formation energies would be manipulated. The concentration of vacancies in a given layered material seems to depend on the chemical gradient across the interface. While the computational work has elucidated oxygen vacancy formation energies for bulk materials, such understanding may not be sufficient to gain complete control over the vacancy concentration.

Near-interface phase stability is another microstructure feature that is gaining interest. Under large interfacial strain, materials can undergo phase transformation, and may lead to the formation of

metastable phases, that may induce novel properties. There are only a handful of studies that have identified structural phase changes; however, it is very likely that this could be a much wider phenomenon especially in interfaces formed by joining two crystallographically dissimilar materials. Both microscopic and theoretical studies are required to develop further understanding. Similarly, the understanding on strain-induced misfit dislocations is at the initial stages. Recent theoretical results are still too contradictory to draw conclusions on the fast ion conducting properties of misfit dislocations. Experimental investigations of oxygen conductivity at misfit dislocations are needed in the near future.

ACKNOWLEDGMENT

This research was supported by the U.S. Department of Energy, Office of Science, Basic Energy Sciences, Materials Science and Engineering Division. The computer simulations were performed at the National Energy Research Scientific Computing Center at Lawrence Berkeley National Laboratory, which is supported by the Office of Science, U.S. Department of Energy under Contract No. DEAC02-05CH11231.

REFERENCES

1. N. Sata, K. Eberman, K. Eberl, and J. Maier: Mesoscopic fast ion conduction in nanometer-scale planar heterostructures. *Nature* **408**(21), 946 (2000).
2. H.Y. Hwang, Y. Iwasa, M. Kawasaki, B. Keimer, N. Nagaosa, and Y. Tokura: Emergent phenomenon at oxide interfaces. *Nat. Mater.* **11**, 103 (2012).
3. A. Ohtomo and H.Y. Hwang: A high-mobility electron gas at the $\text{LaAlO}_3/\text{SrTiO}_3$ heterointerface. *Nature* **427**, 423 (2004).
4. G.S. Rohrer, M. Affatigato, M. Backhaus, R.K. Bordia, H.M. Chan, S. Curtarolo, A. Demkov, J.N. Eckstein, K.T. Faber, J.E. Garay, Y. Gogotsi, L. Huang, L.E. Jones, S.V. Kalinin, R.J. Lad, C.G. Levi, J. Levy, J-P. Maria, L. Mattos, A. Navrotsky, N. Orlovskaya, C. Pantano, J.F. Stebbins, T.S. Sudarshan, T. Tani, K. Scott Weil, and D.J. Green: Challenges in ceramic science: A report from the workshop on emerging research areas in ceramic science. *J. Am. Ceram. Soc.* **95**(12), 3699 (2012).
5. P. Yu, Y-H. Chu, and R. Ramesh: Oxide interfaces: Pathways to novel phenomena. *Mater. Today*. **15**(7-8), 320 (2012).
6. J. Garcia-Barriocanal, A. Rivera-Calzada, M. Varela, Z. Sefrioui, E. Iborra, C. Leon, S.J. Pennycook, and J. Santamaria: Colossal ionic conductivity at interfaces of epitaxial $\text{ZrO}_2: \text{Y}_2\text{O}_3/\text{SrTiO}_3$ heterostructures. *Science* **321**, 676 (2008).
7. A. Rivera-Calzada, M.R. Diaz-Guillen, O.J. Dura, G. Sanchez-Santolino, T.J. Pennycook, R. Schmidt, F.Y. Bruno, J. Garcia-Barriocanal, Z. Sefrioui, N.M. Nemes, M. Garcia-Hernandez, M. Varela, C. Leon, S.T. Pantelides, S.J. Pennycook, and J. Santamaria: Tailoring interface structure in highly strained YSZ/STO heterostructures. *Adv. Mater.* **23**(44), 5268 (2011).
8. S.V. Kalinin and N.A. Spaldin: Functional ion defects in transition metal oxides. *Science* **341**, 858 (2013).
9. R. Ramesh: Complex functional oxide heterostructures. *Curr. Sci.* **105**(8), 1107 (2013).
10. P. Zubko, S. Gariglio, M. Gabay, P. Ghosez, and J-M. Triscone: Interface physics in complex oxide heterostructures. *Annu. Rev. Condens. Matter Phys.* **2**(1), 141 (2011).
11. J. Maier: Nanoionics: Ion transport and electrochemical storage in confined systems. *Nat. Mater.* **4**(11), 805 (2005).
12. F.M. Granozio, G. Koster, and G. Rijnders: Functional oxide interfaces. *MRS Bull.* **38**(12), 1017 (2013).
13. A. Brinkman, M. Huijben, M.V. Zalk, J. Huijben, U. Zeitler, J. Mann, W.V.d. Weil, G. Rijnders, D. Blank, and H. Hilgenkamp: Magnetic effects at the interface between non-magnetic oxides. *Nat. Mater.* **6**(7), 493 (2007).
14. J. Bert, B. Kalisky, C. Bell, M. Kim, Y. Hikita, H. Hwang, and K. Moler: Direct imaging of the coexistence of ferromagnetism and superconductivity at the $\text{LaAlO}_3/\text{SrTiO}_3$ interface. *Nat. Phys.* **7**, 767 (2011).
15. I. Bozovic, G. Logvenov, I. Belca, B. Narimbetov, and I. Sveklo: Epitaxial strain and superconductivity in $\text{La}_{2-x}\text{Sr}_x\text{CuO}_4$ thin films. *Phys. Rev. Lett.* **89**(10), 107001 (2002).
16. D. Fuchs, E. Arac, C. Pinta, S. Schuppler, R. Schneider, and H.V. Löhneysen: Tuning the magnetic properties of LaCoO_3 thin films by epitaxial strain. *Phys. Rev. B.* **77**(1), 014434 (2008).
17. K.J. Choi, M. Biegalski, Y.L. Li, A. Sharan, J. Schubert, R. Uecker, P. Reiche, Y.B. Chen, X.Q. Pan, V. Gopalan, L.Q. Chen, D.G. Schlom, and C.B. Eom: Enhancement of ferroelectricity in strained BaTiO_3 thin films. *Science* **306**, 1005 (2004).
18. C.J. Fennie and K.M. Rabe: Magnetic and electric phase control in epitaxial EuTiO_3 from first principles. *Phys. Rev. Lett.* **97**, 267602, (2006).
19. D.G. Schlom, L-Q. Chen, C.J. Fennie, V. Gopalan, D.A. Muller, X. Pan, R. Ramesh, and R. Uecker: Elastic strain engineering of ferroic oxides. *MRS Bull.* **39**(02), 118 (2014).
20. W. Han, M.J. Demkowicz, N.A. Mara, E. Fu, S. Sinha, A.D. Rollett, Y. Wang, J.S. Carpenter, I.J. Beyerlein, and A. Misra: Design of radiation tolerant materials via interface engineering. *Adv. Mater.* **25**(48), 6975 (2013).
21. X.M. Bai, A.F. Voter, R.G. Hoagland, M. Nastasi, and B.P. Uberuaga: Efficient annealing of radiation damage near grain boundaries via interstitial emission. *Science* **327**, 1631 (2010).
22. I.J. Beyerlein, A. Caro, M.J. Demkowicz, N.A. Mara, A. Misra, and B.P. Uberuaga: Radiation damage tolerant nanomaterials. *Mater. Today* **16**(11), 443 (2013).
23. P.P. Dholabhai, G. Pilania, J.A. Aguiar, A. Misra, and B.P. Uberuaga: Termination chemistry-driven dislocation structure at $\text{SrTiO}_3/\text{MgO}$ heterointerfaces. *Nat. Commun.* **5**, 5043 (2014).
24. K. Koumoto, Y. Wang, R. Zhang, A. Kosuga, and R. Funahashi: Oxide thermoelectric materials: A Nanostructuring approach. *Annu. Rev. Mater. Res.* **40**(1), 363 (2010).
25. J. He, Y. Liu, and R. Funahashi: Oxide thermoelectrics: The challenges, progress, and outlook. *J. Mater. Res.* **26**(15), 1762 (2011).
26. J. Li, Z. Shan, and E. Ma: Elastic strain engineering for unprecedented materials properties. *MRS Bull.* **39**(02), 108 (2014).
27. L. Tarnawska, A. Giussani, P. Zaumseil, M.A. Schubert, R. Paszkiewicz, O. Brandt, P. Storck, and T. Schroeder: Single crystalline $\text{Sc}_2\text{O}_3/\text{Y}_2\text{O}_3$ heterostructures as novel engineered buffer approach for GaN integration on Si (111). *J. Appl. Phys.* **108**(6), 063502 (2010).
28. J.L.M. Rupp, E. Fabbri, D. Marrocchelli, J-W. Han, D. Chen, E. Traversa, H.L. Tuller, and B. Yildiz: Scalable oxygen-ion transport kinetics in metal-oxide films: Impact of thermally induced lattice compaction in acceptor doped ceria films. *Adv. Funct. Mater.* **24**(11), 1562 (2014).

29. H.L. Tuller: Ionic conduction in nanocrystalline materials. *Solid State Ionics* **131**, 143 (2000).
30. E.D. Wachsman and K.T. Lee: Lowering the temperature of solid oxide fuel cells. *Science* **334**, 935 (2011).
31. E. Wachsman, T. Ishihara, and J. Kilner: Low-temperature solid-oxide fuel cells. *MRS Bull.* **39**(09), 773 (2014).
32. J.A. Kilner: Fast oxygen transport in acceptor doped oxides. *Solid State Ionics* **129**, 13 (2000).
33. J.A. Kilner and R.J. Brook: A Study of oxygen ion conductivity in doped non-stoichiometric oxides. *Solid State Ionics* **6**, 237 (1982).
34. I. Stephens and J. Kilner: Ionic conductivity of $Ce_{1-x}Nd_xO_{2-x/2}$. *Solid State Ionics* **177**(7–8), 669 (2006).
35. J.A. Kilner and M. Burriel: Materials for intermediate-temperature solid-oxide fuel cells. *Annu. Rev. Mater. Res.* **44**(1), 365 (2014).
36. P. Knauth and H.L. Tuller: Solid-state ionics: Roots, status, and future prospects. *J. Am. Ceram. Soc.* **85**(7), 1654 (2002).
37. J.B. Goodenough: Oxide-ion electrolytes. *Annu. Rev. Mater. Res.* **33**(1), 91 (2003).
38. S. Hull: Superionics: Crystal structures and conduction processes. *Rep. Prog. Phys.* **67**(7), 1233 (2004).
39. M. Mogensen, N.M. Sammes, and G.A. Tompsett: Physical, chemical and electrochemical properties of pure and doped ceria. *Solid State Ionics* **129**, 63 (2000).
40. H. Inaba and H. Tagawa: Ceria-based solid electrolytes. *Solid State Ionics* **83**, 1 (1996).
41. S.P.S. Badwal: Zirconia-based solid electrolytes: Microstructure, stability and ionic conductivity. *Solid State Ionics* **52**, 23 (1992).
42. L. Minervini, M.I. Zacate, and R.W. Grimes: Defect cluster formation in M_2O_3 -doped CeO_2 . *Solid State Ionics* **116**, 339 (1999).
43. D.A. Andersson, S.I. Simak, N.V. Skorodumova, I.A. Abrikosov, and B. Johansson: Optimization of ionic conductivity in doped ceria. *Proc. Natl. Acad. Sci. U. S. A.* **103**(10), 3518 (2006).
44. S. Omar, E. Wachsman, and J. Nino: Higher conductivity Sm^{3+} and Nd^{3+} co-doped ceria-based electrolyte materials. *Solid State Ionics* **178**(37–38), 1890 (2008).
45. S. Omar, E.D. Wachsman, J.L. Jones, and J.C. Nino: Crystal structure-ionic conductivity relationships in doped ceria systems. *J. Am. Ceram. Soc.* **92**(11), 2674 (2009).
46. D.W. Jung, K.L. Duncan, M.A. Camaratta, K.T. Lee, J.C. Nino, and E.D. Wachsman: Effect of annealing temperature and dopant concentration on the conductivity behavior in $(DyO_{1.5})_x-(WO_3)_y-(BiO_{1.5})_{1-x-y}$. *J. Am. Ceram. Soc.* **95**(3), 1384 (2010).
47. A. Bogicevic, C. Wolverton, G. Crosbie, and E. Stechel: Defect ordering in aliovalently doped cubic zirconia from first principles. *Phys. Rev. B* **64**(1), 014106 (2001).
48. Y. Arachi, H. Sakai, O. Yamamoto, Y. Takeda, and N. Imanishai: Electrical conductivity of the $ZrO_2-Ln_2O_3$ (Ln =lanthanides) system. *Solid State Ionics* **121**, 133 (1999).
49. D.W. Jung, K.L. Duncan, and E.D. Wachsman: Effect of total dopant concentration and dopant ratio on conductivity of $(DyO_{1.5})_x-(WO_3)_y-(BiO_{1.5})_{1-x-y}$. *Acta Mater.* **58**(2), 355 (2010).
50. T. Politova and J.T.S. Irvine: Investigation of scandia–yttria–zirconia system as an electrolyte material for intermediate temperature fuel cells—influence of yttria content in system $(Y_2O_3)_x(Sc_2O_3)_{(11-x)}(ZrO_2)_{89}$. *Solid State Ionics* **168**(1–2), 153 (2004).
51. O. Yamamoto, Y. Arati, Y. Takeda, N. Imanishi, Y. Mizutani, M. Kawai, and Y. Nakamura: Electrical conductivity of stabilized zirconia with ytterbia and scandia. *Solid State Ionics* **79**, 137 (1995).
52. D.S. Aidhy, J.C. Nino, S.B. Sinnott, E.D. Wachsman, and S.R. Phillpot: Vacancy-ordered structure of cubic bismuth oxide from simulation and crystallographic analysis. *J. Am. Ceram. Soc.* **91**(7), 2349 (2008).
53. B. Yildiz: “Stretching” the energy landscape of oxides—Effects on electrocatalysis and diffusion. *MRS Bull.* **39**(02), 147 (2014).
54. A.Y. Borisevich, A.R. Lupini, J. He, E.A. Eliseev, A.N. Morozovska, G.S. Svehnikov, P. Yu, Y.-H. Chu, R. Ramesh, S.T. Pantelides, S.V. Kalinin, and S.J. Pennycook: Interface dipole between two metallic oxides caused by localized oxygen vacancies. *Phys Rev B.* **86**(14), 140102 (2012).
55. Z. Zhong, P.X. Xu, and P.J. Kelly: Polarity-induced oxygen vacancies at $LaAlO_3/SrTiO_3$ interfaces. *Phys Rev B.* **82**(16), 165127 (2010).
56. W. Jiang, M. Noman, Y.M. Lu, J.A. Bain, P.A. Salvador, and M. Skowronski: Mobility of oxygen vacancy in $SrTiO_3$ and its implications for oxygen-migration-based resistance switching. *J. Appl. Phys.* **110**(3), 034509 (2011).
57. D.S. Aidhy, Y. Zhang, and W.J. Weber: (001) $SrTiO_3$ | (001) MgO interface and oxygen-vacancy stability from first-principles calculations. *ACS Appl. Mater. Interfaces* **6**(17), 15536 (2014).
58. D.S. Aidhy, B. Liu, Y. Zhang, and W.J. Weber: Strain-induced phase and oxygen-vacancy stability in ionic interfaces from first-principles calculations. *J. Phys. Chem. C* **118**(51), 30139 (2014).
59. U. Aschauer, R. Pfenninger, S.M. Selbach, T. Grande, and N.A. Spaldin: Strain-controlled oxygen vacancy formation and ordering in $CaMnO_3$. *Phys. Rev. B.* **88**(5), 054111 (2013).
60. A. Ourmazd and J.C.H. Spence: Detection of oxygen ordering in superconducting cuprates. *Nature* **329**(1), 425 (1987).
61. R. Devanathan and W.J. Weber: Dynamic annealing of defects in irradiated zirconia-based ceramics. *J. Mater. Res.* **23**(03), 593 (2011).
62. D.S. Aidhy and D. Wolf: On the response of ionic crystals to irradiation. *Nucl. Technol.* **182**(2), 138 (2013).
63. D. Pergolesi, E. Fabbri, S.N. Cook, V. Roddatis, E. Traversa, and J.A. Kilner: Tensile lattice distortion does not affect oxygen transport in yttria-stabilized zirconia- CeO_2 heterointerfaces. *ACS Nano* **6**(12), 10524 (2012).
64. X. Guo: Can we achieve significantly higher ionic conductivity in nanostructured zirconia? *Scr. Mater.* **65**(2), 96 (2011).
65. G. Knoner, K. Reimann, R. Rower, U. Sodervall, and H.E. Schaefer: Enhanced oxygen diffusivity in interfaces of nanocrystalline $ZrO_2.Y_2O_3$. *Proc. Natl. Acad. Sci. U. S. A.* **100**(7), 3870 (2003).
66. I. Kosacki, C. Rouleau, P. Becher, J. Bentley, and D. Lowndes: Nanoscale effects on the ionic conductivity in highly textured YSZ thin films. *Solid State Ionics* **176**(13–14), 1319 (2005).
67. M. Sillarsen, P. Eklund, N. Pryds, E. Johnson, U. Helmersson, and J. Böttiger: Low-temperature superionic conductivity in strained yttria-stabilized zirconia. *Adv. Funct. Mater.* **20**(13), 2071 (2010).
68. A. Karthikeyan, C.-L. Chang, and S. Ramanathan: High temperature conductivity studies on nanoscale yttria-doped zirconia thin films and size effects. *Appl. Phys. Lett.* **89**(18), 183116 (2006).
69. J. Jiang, X. Hu, W. Shen, C. Ni, and J.L. Hertz: Improved ionic conductivity in strained yttria-stabilized zirconia thin films. *Appl. Phys. Lett.* **102**(14), 143901 (2013).
70. T. Suzuki, I. Koscki, and H.U. Anderson: Microstructure-electrical conductivity relationships in nanocrystalline ceria thin films. *Solid State Ionics* **151**, 111 (2002).
71. H. Huang, T.M. Gur, Y. Saito, and F. Prinz: High ionic conductivity in ultrathin nanocrystalline gadolinia-doped ceria films. *Appl. Phys. Lett.* **89**(14), 143107 (2006).
72. C. Korte, A. Peters, J. Janek, D. Hesse, and N. Zakharov: Ionic conductivity and activation energy for oxygen ion transport in superlattices—the semicoherent multilayer system YSZ ($ZrO_2 + 9.5 \text{ mol\% } Y_2O_3$)/ Y_2O_3 . *Phys. Chem. Chem. Phys.* **10**(31), 4623 (2008).

73. C. Korte, N. Schichtel, D. Hesse, and J. Janek: Influence of interface structure on mass transport in phase boundaries between different ionic materials. *Monatsh. Chem.* **140**(9), 1069 (2009).
74. N. Schichtel, C. Korte, D. Hesse, and J. Janek: Elastic strain at interfaces and its influence on ionic conductivity in nanoscaled solid electrolyte thin films—Theoretical considerations and experimental studies. *Phys. Chem. Chem. Phys.* **11**, 3043 (2009).
75. H. Aydin, C. Korte, and J. Janek: ^{18}O -Tracer diffusion along nanoscaled $\text{Sc}_2\text{O}_3/\text{yttria}$ stabilized zirconia (YSZ) multilayers: On the influence of strain. *Sci. Technol. Adv. Mater.* **14**(3), 035007 (2013).
76. X. Guo, E. Vasco, S. Mi, K. Szot, E. Wachsman, and R. Waser: Ionic conduction in zirconia films of nanometer thickness. *Acta Mater.* **53**(19), 5161 (2005).
77. E. Navickas, M. Gerstl, G. Friedbacher, F. Kubel, and J. Fleig: Measurement of the across-plane conductivity of YSZ thin films on silicon. *Solid State Ionics* **211**, 58 (2012).
78. W. Jung, J.L. Hertz, and H.L. Tuller: Enhanced ionic conductivity and phase meta-stability of nano-sized thin film yttria-doped zirconia (YDZ). *Acta Mater.* **57**(5), 1399 (2009).
79. M. Gerstl, G. Friedbacher, F. Kubel, H. Hutter, and J. Fleig: The relevance of interfaces for oxide ion transport in yttria stabilized zirconia (YSZ) thin films. *Phys. Chem. Chem. Phys.* **15**(4), 1097 (2013).
80. M.G. Bellino, D.G. Lamas, and N.E. Walsøe de Reca: Enhanced ionic conductivity in nanostructured, heavily doped ceria ceramics. *Adv. Func. Mater.* **16**(1), 107 (2006).
81. J. An, J. Bae, S. Hong, B. Koo, Y.-B. Kim, T.M. Gür, and F.B. Prinz: Grain boundary blocking of ionic conductivity in nanocrystalline yttria-doped ceria thin films. *Scr. Mater.* **104**, 45 (2015).
82. K.-R. Lee, J.-H. Lee, and H.-I. Yoo: Grain size effect on the electrical properties of nanocrystalline ceria. *J. Eur. Ceram. Soc.* **34**(10), 2363 (2014).
83. F. Maglia, F. Farina, M. Dapiaggi, I.G. Tredici, and U. Anselmi-Tamburini: Transport properties in bulk nanocrystalline Sm-doped ceria with doping content between 2 and 30at.%. *Solid State Ionics* **225**, 412 (2012).
84. R.A. De Souza, M.J. Pietrowski, U. Anselmi-Tamburini, S. Kim, Z.A. Munir, and M. Martin: Oxygen diffusion in nanocrystalline yttria-stabilized zirconia: The effect of grain boundaries. *Phys. Chem. Chem. Phys.* **10**(15), 2067 (2008).
85. E.C.C. Souza, W.C. Chueh, W. Jung, E.N.S. Muccillo, and S.M. Haile: Ionic and electronic conductivity of nanostructured, samaria-doped ceria. *J. Electrochem. Soc.* **159**(5), K127 (2012).
86. J. Jiang and J.L. Hertz: On the variability of reported ionic conductivity in nanoscale YSZ thin films. *J. Electroceram.* **32**(1), 37 (2013).
87. Z.-P. Li, T. Mori, G.J. Auchterlonie, J. Zou, and J. Drennan: Direct evidence of dopant segregation in Gd-doped ceria. *Appl. Phys. Lett.* **98**(9), 093104 (2011).
88. M. de Ridder, A.G.J. Vervoort, R.G.V. Welzenis, and H.H. Brongersma: The limiting factor for oxygen exchange at the surface of fuel cell electrolytes. *Solid State Ionics* **156**, 255 (2003).
89. Y. Lei, Y. Ito, and N.D. Browning: Segregation effects at grain boundaries in fluorite-structured ceramics. *J. Am. Ceram. Soc.* **85**(9), 2359 (2002).
90. M. Aoki, Y.-M. Chiang, I. Kosacki, J.-R. Lee, H. Tuller, and Y. Liu: Solute segregation and grain-boundary impedance in high-purity stabilized zirconia. *J. Am. Ceram. Soc.* **79**(5), 1169 (1996).
91. H.B. Lee, F.B. Prinz, and W. Cai: Atomistic simulations of surface segregation of defects in solid oxide electrolytes. *Acta Mater.* **58**(6), 2197 (2010).
92. M. Yoshiya and T. Oyama: Impurity and vacancy segregation at symmetric tilt grain boundaries in Y_2O_3 -doped ZrO_2 . *J. Mater. Sci.* **46**(12), 4176 (2011).
93. S. Plimpton: Fast parallel algorithms for short-range molecular dynamics. *J. Comput. Phys.* **117**, 1 (1995).
94. D.S. Aidhy, Y. Zhang, and W.J. Weber: Impact of segregation energetics on oxygen conductivity at ionic grain boundaries. *J. Mater. Chem. A* **2**, 1704 (2014).
95. M. Hong, B.P. Uberuaga, S.R. Phillpot, D.A. Andersson, C.R. Stanek, and S.B. Sinnott: The role of charge and ionic radius on fission product segregation to a model UO_2 grain boundary. *J. Appl. Phys.* **113**(13), 134902 (2013).
96. P.-I. Chen and I.-W. Chen: Grain growth in CeO_2 : Dopant effects, defect mechanism and solute drag. *J. Am. Ceram. Soc.* **79**(7), 1793 (1996).
97. D.S. Aidhy, Y. Zhang, and W.J. Weber: Stabilizing nanocrystalline grains in ceramic-oxides. *Phys. Chem. Chem. Phys.* **15**, 18915 (2013).
98. J. Simon, T. Walther, W. Mader, J. Klein, D. Reisinger, L. Alff, and R. Gross: Diffusion and segregation effects in doped manganite/titanate heterostructures. *Appl. Phys. Lett.* **84**(19), 3882 (2004).
99. S. Estradé, J.M. Rebled, J. Arbiol, F. Peiró, I.C. Infante, G. Herranz, F. Sánchez, J. Fontcuberta, R. Córdoba, B.G. Mendis, and A.L. Bleloch: Effects of thickness on the cation segregation in epitaxial (001) and (110) $\text{La}_{2/3}\text{Ca}_{1/3}\text{MnO}_3$ thin films. *Appl. Phys. Lett.* **95**(7), 072507 (2009).
100. C. Tian and S.-W. Chan: Ionic conductivities, sintering temperatures and microstructures of bulk ceramic CeO_2 doped with Y_2O_3 . *Solid State Ionics* **134**, 89 (2000).
101. Y.M. Chiang, E.B. Lavik, I. Kosacki, H.L. Tuller, and J.Y. Ying: Defect and transport properties of nanocrystalline CeO_{2-x} . *Appl. Phys. Lett.* **69**(2), 185 (1996).
102. K.S. Brinkman, H. Takamura, H.L. Tuller, and T. Iijima: The oxygen permeation properties of nanocrystalline CeO_2 thin films. *J. Electrochem. Soc.* **157**(12), B1852 (2010).
103. A. Kushima and B. Yildiz: Oxygen ion diffusivity in strained yttria stabilized zirconia: Where is the fastest strain? *J. Mater. Chem.* **20**(23), 4809 (2010).
104. H. Ohta, S. Kim, Y. Mune, T. Mizoguchi, K. Nomura, S. Ohta, T. Nomura, Y. Nakanishi, Y. Ikuhara, M. Hirano, H. Hosono, and K. Koumoto: Giant thermoelectric Seebeck coefficient of a two-dimensional electron gas in SrTiO_3 . *Nat. Mater.* **6**(2), 129 (2007).
105. A. Tebano, E. Fabbri, D. Pergolesi, G. Balestrino, and E. Traversa: Room-temperature giant persistent photoconductivity in $\text{SrTiO}_3/\text{LaAlO}_3$ heterostructures. *ACS Nano*. **6**(2), 1278 (2012).
106. J. Su, L. Guo, N. Bao, and C.A. Grimes: Nanostructured $\text{WO}_3/\text{BiVO}_4$ heterojunction films for efficient photoelectrochemical water splitting. *Nano Lett.* **11**(5), 1928 (2011).
107. C.W. Bark, P. Sharma, Y. Wang, S.H. Baek, S. Lee, S. Ryu, C.M. Folkman, T.R. Paudel, A. Kumar, S.V. Kalinin, A. Sokolov, E.Y. Tsymbal, M.S. Rzchowski, A. Gruverman, and C.B. Eom: Switchable induced polarization in $\text{LaAlO}_3/\text{SrTiO}_3$ heterostructures. *Nano Lett.* **12**(4), 1765 (2012).
108. M. Nord, P.E. Vullum, M. Moreau, J.E. Boschker, S.M. Selbach, R. Holmestad, and T. Tybell: Structural phases driven by oxygen vacancies at the $\text{La}_{0.7}\text{Sr}_{0.3}\text{MnO}_3/\text{SrTiO}_3$ hetero-interface. *Appl. Phys. Lett.* **106**(4), 041604 (2015).
109. J. Mannhart and D.G. Schlom: Oxide interfaces—an opportunity for electronics. *Science* **327**(5973), 1607 (2010).
110. J.N. Eckstein: Oxide interfaces: Watch out for the lack of oxygen. *Nat. Mater.* **6**, 473 (2007).

111. D.S. Aidhy, B. Liu, Y. Zhang, and W.J. Weber: Chemical expansion affected oxygen vacancy stability in different oxide structures from first principles calculations. *Comput. Mater. Sci.* **99**, 298 (2015).
112. S.Y. Choi, S.D. Kim, M. Choi, H.S. Lee, J. Ryu, N. Shibata, T. Mizoguchi, E. Tochigi, T. Yamamoto, S.J. Kang, and Y. Ikuhara: Assessment of strain-generated oxygen vacancies using SrTiO₃ bicrystals. *Nano. lett.* **15**(6), 4129 (2015).
113. W. Donner, C. Chen, M. Liu, A.J. Jacobson, Y.-L. Lee, M. Gadre, and D. Morgan: Epitaxial strain-induced chemical ordering in La_{0.5}Sr_{0.5}CoO_{3-δ} films on SrTiO₃. *Chem. Mater.* **23**(4), 984 (2011).
114. M. Fronzi, S. Cereda, Y. Tateyama, A. De Vita, and E. Traversa: Ab initio investigation of defect formation at ZrO₂-CeO₂ interfaces. *Phys. Rev. B.* **86**(8), 085407(1) (2012).
115. J.J. Plata, A.M. Marquez, and J.F. Sanz: Understanding the interplay of dopants, interfaces, and anionic conductivity in doped ceria/zirconia heteroepitaxial structures. *Chem. Mater.* **26** (11), 3385 (2014).
116. T.J. Pennycook, M.J. Beck, K. Varga, M. Varela, S.J. Pennycook, and S.T. Pantelides: Origin of colossal ionic conductivity in oxide multilayers: Interface induced sublattice disorder. *Phys. Rev. Lett.* **104**(11), (2010).
117. T.J. Pennycook, M.P. Oxley, J. Garcia-Barriocanal, F.Y. Bruno, C. Leon, J. Santamaria, S.T. Pantelides, M. Varela, and S.J. Pennycook: Seeing oxygen disorder in YSZ/SrTiO₃ colossal ionic conductor heterostructures using EELS. *Eur. Phys. J. Appl. Phys.* **54**(3), 33507 (2011).
118. S.J. Pennycook, H. Zhou, M.F. Chisholm, A.Y. Borisevich, M. Varela, J. Gazquez, T.J. Pennycook, and J. Narayan: Misfit accommodation in oxide thin film heterostructures. *Acta. Mater.* **61**(8), 2725 (2013).
119. W.L. Cheah and M.W. Finnis: Structure of multilayer ZrO₂/SrTiO₃. *J. Mater. Sci.* **47**(4), 1631 (2012).
120. A. Tarancón and A. Morata: New insights into the origin of the oxide ionic diffusion change in strained lattices of yttria stabilized zirconia. *Comput. Mater. Sci.* **103**, 206 (2015).
121. T.G. Desai and B.P. Uberuaga: Stress-induced phase transformation in nanocrystalline UO₂. *Scr. Mater.* **60**(10), 878 (2009).
122. M. Lang, J. Lian, J. Zhang, F. Zhang, W. Weber, C. Trautmann, and R. Ewing: Single-ion tracks in Gd₂Zr_{2-x}Ti_xO₇ pyrochlores irradiated with swift heavy ions. *Phys. Rev. B.* **79**(22), 224105 (2009).
123. M. Lang, F. Zhang, J. Zhang, J. Wang, J. Lian, W.J. Weber, B. Schuster, C. Trautmann, R. Neumann, and R.C. Ewing: Review of A₂B₂O₇ pyrochlore response to irradiation and pressure. *Nucl. Instrum. Methods Phys. Res., Sect. B* **268**(19), 2951 (2010).
124. D.S. Aidhy, R. Sachan, E. Zarkadoula, O. Pakarinen, M. Chisholm, Y. Zhang, and W.J. Weber: Fast ion conductivity in strained defect-fluorite structure created by ion tracks in Gd₂Ti₂O₇. *Sci. Rep.* **5**, 16297, doi:10.1038/srep16297 (2015).
125. P.J. Wilde and C.R.A. Catlow: Molecular dynamics study of the effect of doping and disorder on diffusion in gadolinium zirconate. *Solid State Ionics* **112**, 185 (1998).
126. A. Kalabukhov, R. Gunnarsson, J. Börjesson, E. Olsson, T. Claesson, and D. Winkler: Effect of oxygen vacancies in the SrTiO₃ substrate on the electrical properties of the LaAlO₃/SrTiO₃ interface. *Phys. Rev. B.* **75**, 121404 (2007).
127. Y. Zhu, C. Song, A.M. Minor, and H. Wang: Cs-corrected scanning transmission electron microscopy investigation of dislocation core configurations at a SrTiO₃/MgO heterogeneous interface. *Microsc. Microanal.* **19**(3), 706 (2013).
128. W. Li, W. Zhang, L. Wang, J. Gu, A. Chen, R. Zhao, Y. Liang, H. Guo, R. Tang, C. Wang, K. Jin, H. Wang, and H. Yang: Vertical interface induced dielectric relaxation in nanocomposite (BaTiO₃)_{1-x}:(Sm₂O₃)_x thin films. *Sci. Rep.* **5**, 11335 (2015).
129. H. Zhou, M.F. Chisholm, P. Pant, H.J. Chang, J. Gazquez, S.J. Pennycook, and J. Narayan: Atomic structure of misfit dislocations in nonpolar ZnO/Al₂O₃ heterostructures. *Appl. Phys. Lett.* **97**(12), 121914 (2010).
130. A. Herpers, K.J. O'Shea, D.A. MacLaren, M. Noyong, B. Rösger, U. Simon, and R. Dittmann: Competing strain relaxation mechanisms in epitaxially grown Pr_{0.48}Ca_{0.52}MnO₃ on SrTiO₃. *APL Mater.* **2**(10), 106106 (2014).
131. D. Marrocchelli, L. Sun, and B. Yildiz: Dislocations in SrTiO₃: Easy to reduce but not so fast for oxygen transport. *J. Am. Chem. Soc.* **137**(14), 4735 (2015).
132. V. Metlenko, A.H. Ramadan, F. Gunkel, H. Du, H. Schraknepper, S. Hoffmann-Eifert, R. Dittmann, R. Waser, and R.A. De Souza: Do dislocations act as atomic autobahns for oxygen in the perovskite oxide SrTiO₃? *Nanoscale* **6**(21), 12864 (2014).
133. L. Sun, D. Marrocchelli, and B. Yildiz: Edge dislocation slows down oxide ion diffusion in doped CeO₂ by segregation of charged defects. *Nat. Commun.* **6**, 6294 (2015).
134. S.T. Murphy, E.E. Jay, and R.W. Grimes: Pipe diffusion at dislocations in UO₂. *J. Nucl. Mater.* **447**(1-3), 143 (2014).
135. Y. Lin, S. Fang, D. Su, K.S. Brinkman, and F. Chen: Enhancing grain boundary ionic conductivity in mixed ionic-electronic conductors. *Nat. Commun.* **6**, 6824 (2015).
136. J. Jiang, W. Shen, and J.L. Hertz: Structure and ionic conductivity of nanoscale gadolinia-doped ceria thin films. *Solid State Ionics* **249-250**, 139 (2013).
137. Y. Shi, A.H. Bork, S. Schweiger, and J.L. Rupp: The effect of mechanical twisting on oxygen ionic transport in solid-state energy conversion membranes. *Nat. Mater.* **14**(7), 721 (2015).